UCLA
UCLA Previously Published Works

Title

An Antimicrobial Dental Light Curable Bioadhesive Hydrogel for Treatment of Peri-Implant Diseases

Permalink

https://escholarship.org/uc/item/88b4t3pn

Journal

Matter, 1(4)

ISSN

2590-2393

Authors

Sani, Ehsan Shirzaei
Lara, Roberto Portillo
Aldawood, Zahra
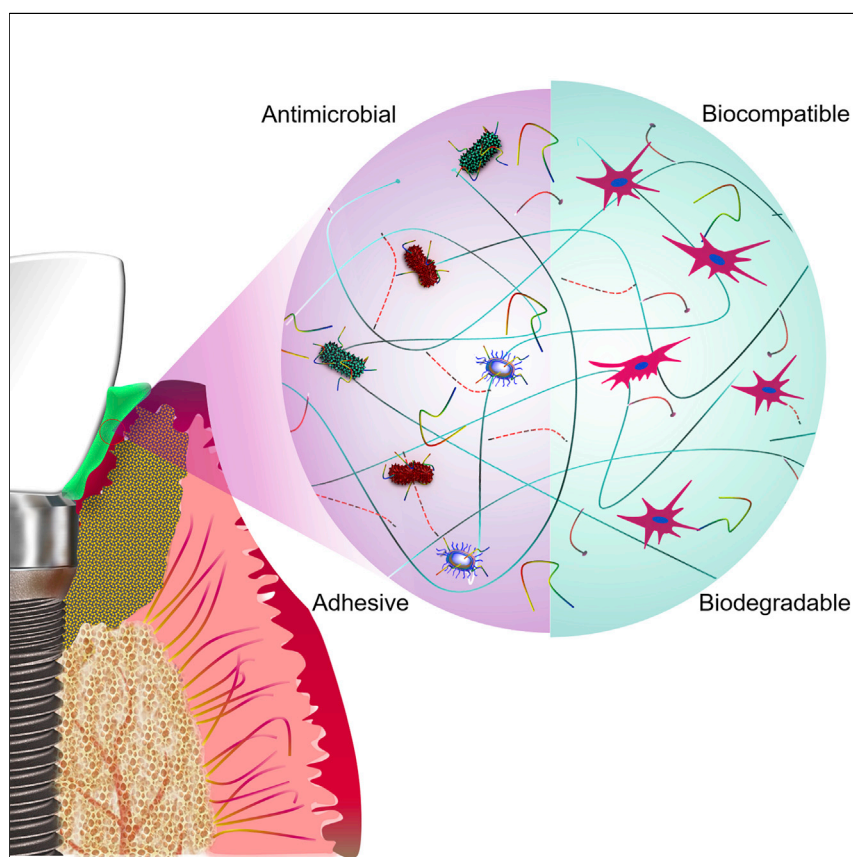et al.

Publication Date

2019-10-01

DOI

10.1016/j.matt.2019.07.019

Peer reviewed

Article

An Antimicrobial Dental Light Curable Bioadhesive Hydrogel for Treatment of Peri-Implant Diseases

Dental implants are the current solution for replacement of missing teeth. However, the majority of patients with implants suffer from implant diseases caused by microbial infection and bone loss. There is an unmet need for the treatment of dental diseases. We developed a safe, cheap, and fast applicable glue with antimicrobial properties, designed for the treatment of periodontal diseases. This material can be delivered in liquid form around the implant and solidified by using a dental light to prevent infection and promote bone healing.

Ehsan Shirzaei Sani, Roberto Portillo Lara, Zahra Aldawood, ..., Alpdogan Kantarci, Giuseppe Intini, Nasim Annabi

nannabi@ucla.edu

HIGHLIGHTS

A visible-light crosslinkable hydrogel for treatment of periodontal diseases

High adhesion to soft/hard tissues and implant surfaces

High antimicrobial properties against periodontal pathogenic bacteria

A versatile platform for autologous bone growth *in vivo*

4

Demonstrate
Proof-of-concept of performance with intended application/response

Article

An Antimicrobial Dental Light Curable Bioadhesive Hydrogel for Treatment of Peri-Implant Diseases

Ehsan Shirzaei Sani,[1] Roberto Portillo Lara,[2] Zahra Aldawood,[3] Seyed Hossein Bassir,[3,4] Daniel Nguyen,[5] Alpdogan Kantarci,[5] Giuseppe Intini,[6,7,8] and Nasim Annabi[1,9,10,11,]*

SUMMARY

Dental implants remain the standard of care to replace missing teeth, which has led to an increase in the number of patients affected by peri-implant diseases (PIDs). Here, we report the development of an antimicrobial bioadhesive, GelAMP, for the treatment of PIDs. The hydrogel is based on a visible-light-activated naturally derived polymer (gelatin) and an antimicrobial peptide (AMP). The optimized formulation of GelAMP could be rapidly crosslinked using commercial dental curing systems. When compared with commercial adhesives, GelAMP exhibited significantly higher adhesion to physiological tissues and titanium surfaces. Moreover, the bioadhesive showed high cytocompatibility and could efficiently promote cell proliferation and migration *in vitro*. GelAMP also showed remarkable antimicrobial activity against *Porphyromonas gingivalis*. Furthermore, it could support the growth of autologous bone after sealing calvarial bone defects in mice. Overall, GelAMP could be used as a platform for the development of more effective therapies against PIDs.

INTRODUCTION

As dental implants have become the standard of care for the replacement of missing teeth, the number of patients affected by peri-implant diseases (PIDs) is increasing.[1] According to their clinical manifestations, PIDs can be mainly categorized in peri-implant mucositis (PIM) and peri-implantitis (PI).[2] PIM refers to a reversible inflammatory process that affects the soft tissues surrounding an implant, resulting in bleeding on gentle probing and, in some cases, suppuration, erythema, and swelling.[2] The etiology of PIM is the bacterial accumulation and biofilm formation around the dental implant.[3] On the other hand, PI presents not only with inflammation of the soft tissues but is also accompanied by a progressive bone loss that could lead to implant failure.[4] Clinical data have shown that progression from PIM to PI is strongly associated with lack of preventive maintenance; thus, opportune treatment of PIM could prevent the progression to PI.[5]

Currently, PIM can be treated with nonsurgical procedures, which include mechanical debridement, alone or in combination with local delivery of antibiotics such as Arestin (minocycline HCl), Elyzol (metronidazole 25%), and Atridox (doxycycline hyclate 10%), which can be injected directly into the sulcus or peri-implant pockets.[6,7] However, because of their inability to efficiently antagonize the infection,[8] the therapeutic efficacy of these approaches is limited.[9] In addition, local and systemic administration of antibiotics may result in hypersensitivity reactions in allergic patients, as well as the development of antibiotic-resistant strains of pathogenic

Progress and Potential

Clinical management of peri-implant diseases (PIDs) constitutes significant challenges. Here, we report a multi-functional adhesive hydrogel with antimicrobial properties for treatment of PIDs. The hydrogel precursor can be crosslinked in seconds using commercially available dental curing systems and forms a hydrogel that can adhere to both soft tissues (gingiva) and hard tissues (dental implants/bone). The hydrogel was extensively characterized *in vitro*, *ex vivo*, and *in vivo*. The engineered adhesive has high adhesion, mechanical stability, cytocompatibility, antimicrobial properties, biodegradability, and bone-regenerative capacity. Overall, this antimicrobial hydrogel adhesive could be used as a minimally invasive platform for the development of more effective therapeutic strategies against PIDs.

bacteria.[10,11] Moreover, as the number of dental implants being placed has continued to increase worldwide; it is predicted that PIDs will become one of the most prominent dental diseases of the future.[3] Therefore, there is a need for more effective therapeutic strategies that could be used to prevent bacterial growth and promote healing around dental implants for the treatment of PIDs.

Current treatments against PIM are mainly aimed at eradicating subgingival dysbiosis and restoring homeostasis to microbial communities in the oral cavity.[12] However, clinical data have shown that nonsurgical mechanical approaches, aimed at disinfection of the affected area, often fail due to recolonization of the periodontal or peri-implant pockets by pathogenic bacteria that perpetuate the disease.[12,13] Moreover, bacterial infection and the subsequent epithelial cell death lead to the release of inflammatory cytokines and chemotactic bacterial peptides, which attract migratory neutrophils. This can worsen implant prognosis, mainly because neutrophil degranulation due to bacterial overload releases tissue-degrading enzymes into the gingival crevice that lead to further tissue trauma.[14,15] As inflammation extends from the marginal gingiva into the supporting periodontal tissues, PIM could eventually progress to PI and lead to bone loss and implant failure. Therefore, therapeutic strategies that efficiently isolate the affected area to prevent the infiltration of bacteria and other unwanted cells, while also enabling the growth of bone-competent cells (i.e., compartmentalized tissue healing), could improve the clinical outcome of patients with PIDs.[16,17]

Periodontal regeneration requires the hierarchical and coordinated response of a variety of soft and hard tissues (i.e., periodontal ligament, gingiva, cementum, and bone) during the wound-healing process.[18] In recent years, clinical evidence has shown that treatment options based on resorbable and non-resorbable membranes could be used for guided tissue regeneration of the periodontal tissues affected by PIDs.[19] Current third-generation membranes are developed not only to act as passive barriers but also as delivery vehicles for the release of specific antibiotics and growth factors.[20,21] Moreover, local delivery yields higher local concentrations of the therapeutic agents, which increases the effectiveness at the site and decreases the risk of systemic side effects. However, several limitations remain pertaining to the unpredictability of the efficacy of these treatments and the need for the delivery of multiple biological mediators to promote tissue regeneration.[22,23]

Hydrogel-based bioadhesives hold remarkable potential for soft- and hard-tissue engineering applications due to their tunable composition and physical properties. The precise control over the microarchitecture, mechanical properties, and degradation rate of hydrogels make them useful alternatives for the controlled delivery of a variety of therapeutic agents *in vivo*. For instance, our group has previously reported the development of antimicrobial hydrogel adhesives for the treatment of chronic nonhealing wounds[24] and orthopedic applications,[25] which were based on extracellular matrix (ECM)-derived biopolymers. In the field of regenerative dentistry, previous studies have reported the engineering of hydrogels based on the combination of alginate with the soluble and insoluble fractions of the dentin matrix.[26] More recently, other groups have developed cell-laden gelatin-based hydrogels that could be photopolymerized using dental curing lights.[27] However, to the best of our knowledge, the development of antimicrobial hydrogels that can strongly adhere to hard and soft oral surfaces for the treatment of PIDs has not been reported.

Here, we describe the development of a visible-light crosslinkable antimicrobial hydrogel adhesive for the treatment of PIDs. This bioadhesive was engineered through

[1]Chemical and Biomolecular Engineering Department, University of California – Los Angeles, Los Angeles, CA 90095, USA

[2]Tecnologico de Monterrey, Escuela de Ingeniería y Ciencias, Zapopan JAL 44-49, Mexico

[3]Department of Oral Medicine, Infection, and Immunity, Harvard School of Dental Medicine, Boston, MA 02115, USA

[4]Department of Periodontology, School of Dental Medicine, Stony Brook University, Stony Brook, NY 11794, USA

[5]Department of Applied Oral Sciences, The Forsyth Institute, Cambridge, MA 02142, USA

[6]Department of Periodontics and Preventive Dentistry, University of Pittsburgh, School of Dental Medicine, Pittsburgh, PA 15213, USA

[7]McGowan Institute for Regenerative Medicine, University of Pittsburgh, Pittsburgh, PA 15213, USA

[8]Harvard Stem Cell Institute, Harvard University, Cambridge, MA 02115, USA

[9]Center for Minimally Invasive Therapeutics (C-MIT), California NanoSystems Institute (CNSI), University of California – Los Angeles, Los Angeles, CA 90095, USA

[10]Harvard-MIT Division of Health Sciences and Technology, Massachusetts Institute of Technology, Cambridge, MA 02139, USA

[11]Lead Contact

*Correspondence: nannabi@ucla.edu

the incorporation of a cationic antimicrobial peptide (AMP) (Tet213) into a photo-crosslinkable gelatin methacryloyl hydrogels to form gelatin methacryloyl-antimicrobial peptide (GelAMP) bioadhesives. We characterized the physical and adhesive properties of the bioadhesives *in vitro*. We also evaluated the antimicrobial properties of the bioadhesives against *Porphyromonas gingivalis*, a Gram-negative bacterium that is involved in the pathogenesis of PIDs. The cytocompatibility of GelAMP was also evaluated *in vitro* via two-dimensional (2D) surface seeding and three-dimensional (3D) encapsulation of W-20-17 murine fibroblasts. Lastly, we evaluated the ability of the bioadhesives to support bone regeneration *in vivo* using a calvarial defect model in mice. The engineered antimicrobial bioadhesives could constitute an effective approach to prevent bacterial growth while also supporting tissue regeneration for the treatment of PIDs.

RESULTS AND DISCUSSION

Synthesis and Physical Characterization of the Bioadhesive Hydrogels

The GelAMP bioadhesives were synthesized based on the combination of biocompatible photoinitiators (triethanolamine [TEA]/*N*-vinyl caprolactam [VC]/Eosin Y), a naturally derived gelatin-based biopolymer (gelatin methacryloyl), and an AMP (Tet213). Type I or cleavage-type initiators are widely used in tissue engineering and are designed to be activated within the range of UV wavelength (i.e., 360–400 nm). However, exposure to UV light could lead to cell damage,[28] impair cellular function,[29] and even lead to neoplasia and cancer.[30] Moreover, only a few type I photoinitiators such as 2-hydroxy-4′-(2-hydroxyethoxy)-2-methylpropiophenone (Irgacure-2959) and lithium phenyl-2,4,6-trimethylbenzoylphosphinate (LAP) have been shown to be cytocompatible at low concentrations.[30–32] Irgacure-2959 has low water solubility and cannot be activated with visible light since its molar absorptivity is limited in the visible-light range (wavelengths >400 nm). Although LAP has high water solubility and cytocompatibility, its highest molar absorbance is in UV-range wavelengths (365–385 nm, $\epsilon \approx 150$–$230\,M^{-1}\,cm^{-1}$), which limits its activation in the visible-light range ($\epsilon \approx 30\,M^{-1}\,cm^{-1}$ at 405 nm).[33] Considering the effective wavelength of Food and Drug Administration (FDA)-approved dental curing light systems (420–480 nm), cleavage-type photoinitiators have limited potential to be used with these platforms in the clinical setting. To address these limitations, we used a visible-light-activated photoinitiator, Eosin Y, which is known as type II or noncleavage-type photoinitiator. This photoinitiator not only can minimize the safety concerns associated with UV light, but also can be rapidly activated with wavelengths (420–480 nm, $\epsilon > 50{,}000\,M^{-1}\,cm^{-1}$) produced by commercial dental curing systems.[33,34] TEA and VC were used as a co-initiator and a co-monomer respectively, to assist free radical photoinitiation.[34]

Hydrogels were synthesized using the highly cytocompatible and visible-light-activated polymer gelatin methacryloyl, a chemically modified form of hydrolyzed collagen that possesses a high number of cell-binding motifs and matrix-metalloproteinase (MMP) degradation sites.[31] These characteristics are critical to ensure proper cell attachment and colonization of the scaffold. Lastly, we incorporated AMP Tet213 into the bioadhesive precursor to impart antimicrobial properties to the hydrogels. AMPs do not readily lead to the selection of resistant mutants and are effective at very low concentrations, which makes them ideal candidates to prevent bacterial growth in biomedical implants via local delivery.[35] To form the antimicrobial GelAMP bioadhesives, we dissolved the gelatin methacryloyl prepolymer at various concentrations (7% and 15%) in a photoinitiator solution containing Tet213 (0.2% [w/v], or 1.34 mM) and photocrosslinked using a dental curing light (420–480 nm) (Figure 1A).
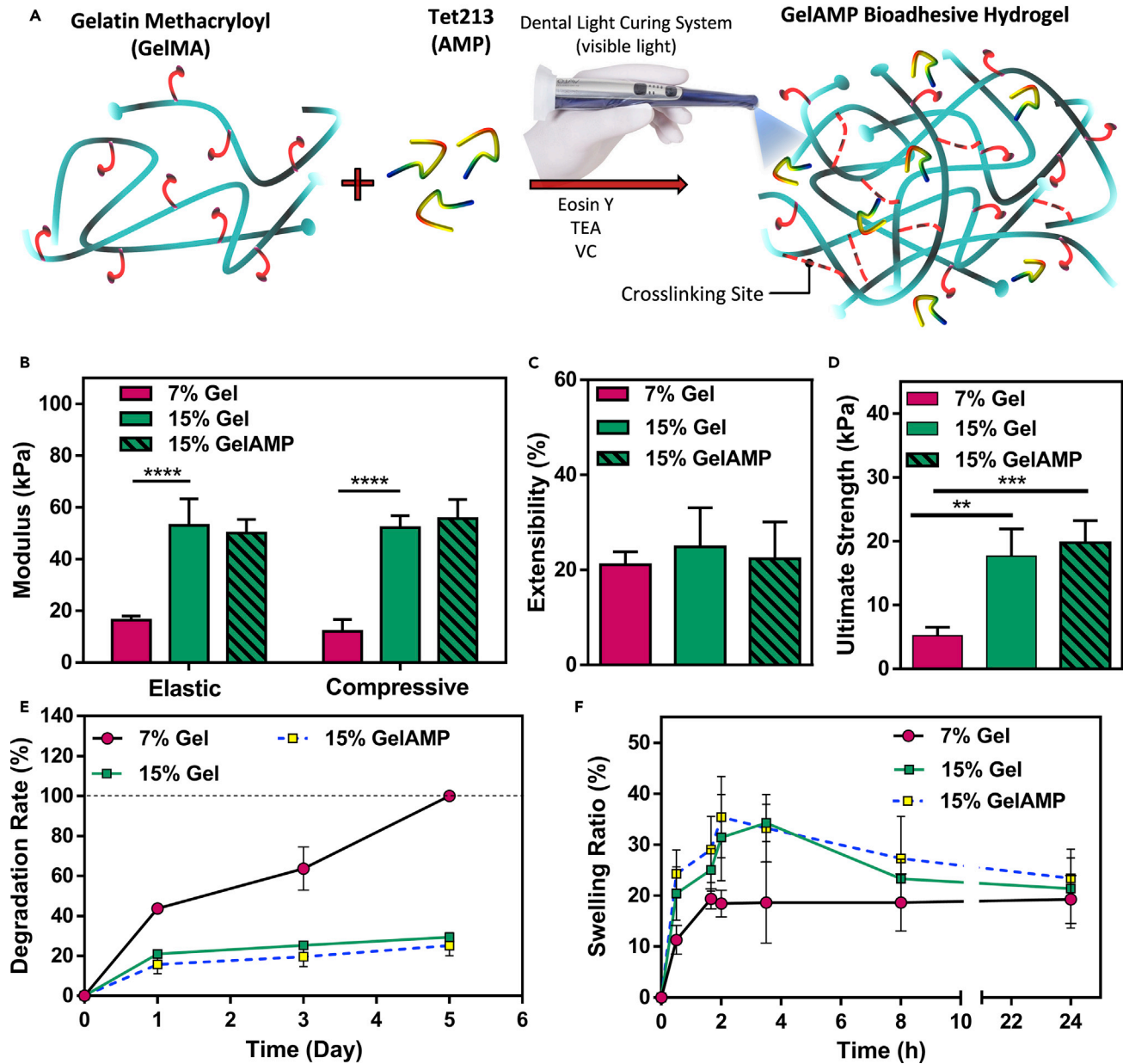
Figure 1. Physical Characterization of the Bioadhesive Hydrogels

(A) Synthesis and photocrosslinking process of the bioadhesive hydrogels.

(B–D) Elastic and compressive modulus (B), extensibility (C), and ultimate stress (D) of the adhesive hydrogels produced by using 7% and 15% (w/v) total polymer concentration with and without AMP.

(E and F) *In vitro* degradation properties in 20 μg/mL collagenase type II solution in Dulbecco's phosphate-buffered saline (DPBS) (E) and swelling ratios in DPBS for 7% and 15% (w/v) adhesive hydrogels with and without AMP (F).

Data are presented as mean ± SD (**p < 0.01, ***p < 0.001, ****p < 0.0001; n ≥ 5).

Control hydrogels (Gel) were formed using a similar technique, but without incorporation of AMP.

To evaluate the physical properties of the bioadhesives, we synthesized hydrogel formulations based on two different concentrations of bioadhesive (7% and 15% [w/v]) with and without incorporation of AMP. Our results showed that 15% (w/v)

bioadhesive hydrogels exhibited a 4.3-fold and 3.2-fold increase in the compressive and elastic moduli, respectively, when compared with 7% (w/v) hydrogels (Figure 1B). In addition, the extensibility of the bioadhesives did not change by changing the concentration of bioadhesive from 7% to 15% (w/v) or by the addition of AMP (Figure 1C). However, the ultimate tensile strength of hydrogels increased from 5.2 ± 1.3 kPa to 19.8 ± 3.5 kPa as the bioadhesive concentration was increased from 7% to 15% (w/v) (Figure 1D). The results also showed that the addition of AMP did not alter the mechanical properties of the bioadhesives, which could be due to the low concentration and the small size of the AMP.[24]

Next, we examined the *in vitro* stability of the bioadhesives by incubating them in collagenase type II solution in Dulbecco's phosphate-buffered saline (DPBS) (20 μg/mL) for 5 days. Bioadhesives with 7% (w/v) concentration resulted in significantly accelerated degradation as compared with bioadhesives with 15% (w/v) concentration. In particular, the 7% (w/v) bioadhesive showed 100.0% degradation at day 5 post incubation, while only 29.4% ± 2.2% of the hydrogel with 15% (w/v) concentration was degraded during the same time (Figure 1E). In addition, there was no significant difference in the degradation of bioadhesive hydrogels with or without AMP (Figure 1E).

The *in vivo* biodegradation of GelAMP bioadhesive was also confirmed in a rat subcutaneous implantation model. Accordingly, hematoxylin and eosin (H&E) analysis of the explanted samples revealed a significant deformation and biodegradation of hydrogels after 56 days of implantation when compared with day 7 (Figure S4). This can be mainly due to the enzymatic hydrolysis of the gelatin backbone.[25]

We then determined the water uptake capacity of the hydrogels by calculating the swelling ratios of the bioadhesives at different concentrations and time points. For this, the swelled weights of the samples after incubation at 37°C in DPBS were divided by their corresponding dry weights. As shown in Figure 1F, the swelling ratios of the hydrogels decreased by increasing bioadhesive concentrations. However, the swelling ratios barely changed after 10 h of incubation, indicating that the equilibrium states were achieved at this time point. In addition, the incorporation of AMP did not alter the degradation rate and the swellability of the bioadhesives (Figures 1E and 1F). Overall, bioadhesives with 15% (w/v) concentration showed higher mechanical stiffness and slower degradation rates compared with 7% (w/v) hydrogels. Previous studies have also investigated the effects of physical properties and microstructural features of hydrogel scaffolds on the regeneration and repair of target tissues.[24,36] An ideal bioadhesive used in the setting of the oral cavity should be elastic and flexible, as well as sufficiently strong to withstand breakage due to the intrinsic dynamism of the oral tissues.[37] For this purpose, the water uptake capacity of the bioadhesives should be finely tuned to prevent excessive swelling, which could lead to patient discomfort and detachment from the wet and highly motile oral tissues. Furthermore, fast degradation of the adhesive could compromise adequate retention and greatly limit their clinical efficacy.[24] Our results showed that, in addition to the higher modulus (Figure 1B) and ultimate strength (Figure 1D) of the 15% (w/v) bioadhesives, they also showed comparatively higher structural stability *in vitro*. This was demonstrated by their slower degradation rates (Figure 1E) and similar swelling equilibrium states upon incubation in DPBS (Figure 1F) when compared with 7% (w/v) bioadhesives. Next, we evaluated the adhesive properties of the hydrogels to soft physiological tissues and hard implant surfaces.
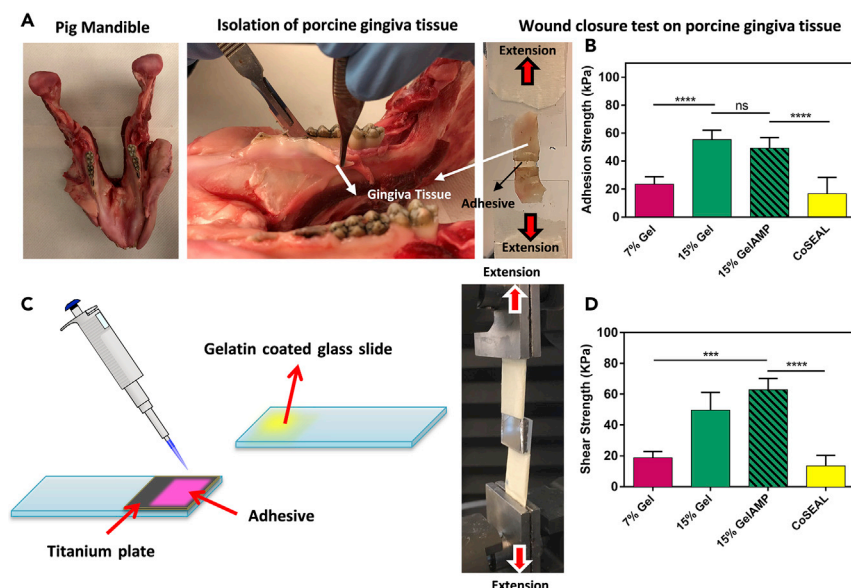
Figure 2. In Vitro and Ex Vivo Adhesion Properties of the Bioadhesive Hydrogels

(A and B) Representative images of (A) wound closure test using pig gingiva tissue based on ASTM standard test (F2458-05) and (B) adhesion strength of the bioadhesive hydrogels and a commercially available adhesive (CoSEAL) to porcine gingiva.

(C) Schematic of the *in vitro* lap shear test based on a modified ASTM standard (F2255-05), using titanium as a substrate.

(D) The *in vitro* lap shear strength of the bioadhesive hydrogels at 7% and 15% polymer concentration and a commercially available adhesive (CoSEAL).

Data are presented as mean $\pm$ SD (ns, not significant; ***$p < 0.001$, ****$p < 0.0001$; n $\geq$ 5).

In Vitro and Ex Vivo Characterization of the Adhesive Properties

The strong retention and adhesion of biomaterials to both the native tissue and the implant surface is a critical factor in promoting periodontal tissue repair and regeneration.[38] Moreover, the designed bioadhesive must withstand the shear and the pressure exerted by the underlying tissues and the high motility of the oral tissues. To evaluate these parameters, we performed standard *in vitro* adhesion tests including wound closure (ASTM F2458-05), lap shear (ASTM F2255-05), and burst pressure (ASTM F2392-04) to assess the adhesiveness of the hydrogels to physiological tissues and titanium surfaces. Similar tests were also performed using a commercially available sealant, CoSEAL, as control. Wound closure tests were performed to measure the adhesive strength of the bioadhesives to soft tissues including porcine gingiva (Figures 2A and 2B) and porcine skin (Figure S1). The results of the wound closure tests revealed that the adhesive strength of the hydrogel to gingiva increased from 23.5 $\pm$ 5.4 kPa to 55.3 $\pm$ 6.7 kPa, by increasing the hydrogel concentration from 7% to 15% (w/v) (Figure 2B). Similarly, the adhesive strength of the bioadhesives to porcine skin was increased 2.1-fold by increasing the total polymer concentration from 7% to 15% (w/v) (Figure S1). Moreover, the presence of AMP did not alter the adhesion strength of the hydrogels for both porcine gingiva and skin tissues (Figures 2B and S1). Lastly, the adhesive strength of the 15% (w/v) bioadhesive was significantly higher than that of CoSEAL, with a 3.3-fold difference for gingiva tissue and a 1.7-fold difference for skin tissue (Figures 2B and S1).

Similar to the wound closure tests, 15% (w/v) bioadhesives, with and without AMP, showed significantly higher lap shear strength to titanium surface as compared

with CoSEAL (i.e., 3.7- and 4.6-fold difference, respectively) (Figure 2D). However, the lap shear strength did not significantly change for 15% (w/v) bioadhesives with and without AMP (Figure 2D). In contrast, the burst pressure of the bioadhesives was increased from 17.0 ± 2.9 kPa at 7% (w/v) to 34.6 ± 4.0 kPa at 15% (w/v) final polymer concentration. Furthermore, the highest burst pressure was observed for 15% (w/v) hydrogels (37.7 ± 6.5 kPa), which was significantly higher than that of CoSEAL (1.7 ± 0.1 kPa) (Figure S2).

Different hydrogel adhesives have been used for sealing, reconnecting tissues, or as implant coatings.[38,39] However, their poor mechanical properties and adhesion to wet tissues have limited their implementation in the clinic. Moreover, the majority of the commercially available dental adhesives are based on polymethyl methacrylate- or acrylic-based resins, which are mainly used as fillers for dentin cavities. Although these types of adhesives have shown strong adhesion and binding to the oral surfaces and tissues (i.e., gingiva and pulpal walls), their potential as a platform for the treatment of PIDs is limited.[40,41] This is mainly due to the lack of cell-binding sites and poor tissue biointegration, which ultimately limit the regenerative capacity of these resins.[41] In contrast, our results revealed that our visible-light curable bioadhesives are able to bind strongly to both hard (titanium) and soft (gingiva tissue) surfaces and withstand high shear stress and pressure. In addition, we have previously shown that gelatin-based bioadhesives can strongly adhere to wet and dynamic tissues such as the lung.[31] Therefore, these bioadhesives could be used to effectively adhere to periodontal tissues, as well as under palatal pressure and during mastication. Moreover, due to the high regenerative capacity of ECM-derived biopolymers, gelatin-based bioadhesives could constitute a suitable alternative for the treatment of PIDs.[24]

In Vitro Evaluation of the Antimicrobial Properties of the Bioadhesives

AMPs are composed of short sequences of cationic amino acids, which have been shown to possess broad-spectrum bactericidal activity against both normal and antibiotic-resistant bacteria.[24,35] AMPs bind to the negatively charged outer leaflet of bacterial cell membranes, which leads to changes in bacterial surface electrostatics, increased membrane permeabilization, and cell lysis.[24]

Here, we synthesized GelAMP, a dental light curable bioadhesive with antimicrobial properties through the incorporation of AMP into bioadhesive hydrogels. Previously, we have shown that AMP Tet213 at very low concentrations is effective against both Gel (+/−) bacteria.[24] Here, we used an optimized concentration of AMP in this work (0.2% [w/v]) based on our previous study.[24] First, we evaluated the antimicrobial activity of the resulting bioadhesive against *P. gingivalis* using a standard colony-forming units (CFU) assay and direct visualization of the bacteria-laden hydrogels via scanning electron microscopy (SEM) (Figure 3). The CFU assay showed that the number of *P. gingivalis* colonies in the 3-logarithmic dilution decreased from 37.7 ± 3.5 at 0.0% (w/v) AMP to 10.6 ± 1.9 at 0.2% (w/v) AMP (Figures 3A and 3B). A similar response was also observed for the 4-logarithmic dilution, which further confirmed the bactericidal properties of the engineered antimicrobial GelAMP bioadhesives when compared with pristine hydrogels as control (Figure 3B). SEM micrographs also showed that the hydrogels without AMP exhibited significant bacterial infiltration and colonization throughout the polymer network (Figure 3C). In contrast, GelAMP containing 0.2% (w/v) AMP showed high antimicrobial activity as demonstrated by the complete absence of bacterial clusters on both surface and cross-sections of the bioadhesives (Figure 3D).
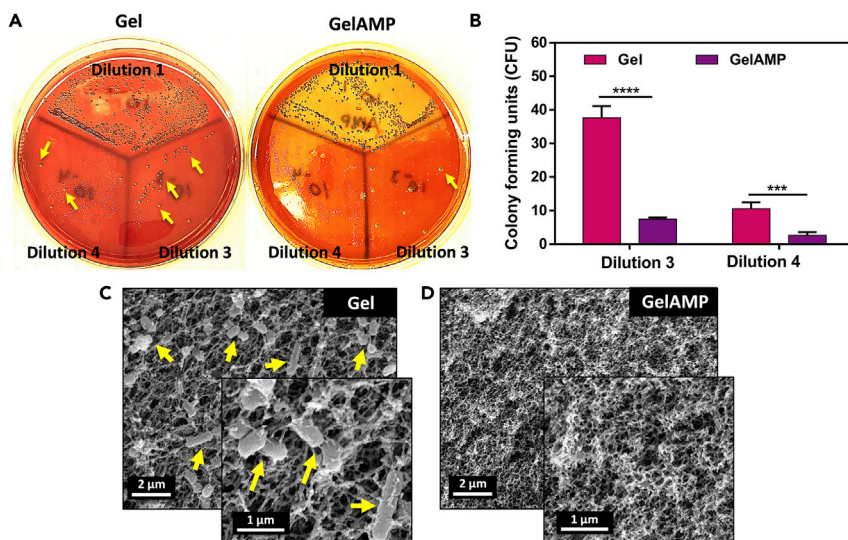
Figure 3. *In Vitro* **Antibacterial Properties of the Bioadhesive Hydrogels against** *P. gingivalis*
(A) Representative images of *P. gingivalis* colonies grown on blood agar plates for bioadhesives with and without AMP (Dilution 1, 3 and 4 represent 1-, 3-, and 4-logarithmic dilutions, respectively). (B–D) Quantification of colony-forming units (CFU) for bioadhesive hydrogels with and without AMP (0.2% [w/v] or 1.34 mM), seeded with *P. gingivalis* bacteria (day 4) (B). Representative SEM images of *P. gingivalis* colonization on bioadhesive hydrogels containing (C) 0% and (D) 0.2% (w/v) AMP. Clusters of bacteria are indicated by yellow arrows (scale bars: 1 and 2 μm).
***p < 0.001, ****p < 0.0001.

A variety of AMPs such as defensins and cathelicidins are normally found in the oral cavity, particularly in the gingival crevicular fluid and in salivary secretions, and constitute the first line of defense against bacterial infection.[42] Moreover, AMPs do not trigger resistance mechanisms, and play a key role in the regulation of microbial homeostasis and the progression of gingival and periodontal diseases.[43] Because of this, previous groups have explored the use of AMPs as active coatings for dental implants and other therapeutic strategies aimed at the prevention of bacterial infection.[44,45] However, AMPs are highly susceptible to proteolytic degradation by proteases secreted by bacteria and host cells and, thus, efficient *in vivo* delivery of AMPs to the site of infection remains challenging. Thus, the engineered bioadhesives in this work could be used to protect AMPs from environmental degradation and to deliver physiologically relevant concentrations of AMPs for controlled periods of time.

Cell Studies
An ideal bioadhesive not only must be cytocompatible but should also allow the attachment and proliferation of cells within the 3D microstructure to support biointegration and healing. Here, we assessed the ability of the engineered bioadhesives to support the attachment and proliferation of migratory cells from the bone stroma via 3D encapsulation of bone marrow stromal cells (Figure 4). In addition, we evaluated the ability of the bioadhesives to support the growth and proliferation of migratory stromal cells via 3D encapsulation of freshly isolated calvarial bone sutures.

In Vitro Cytocompatibility and Proliferation of 3D Encapsulated Cells within the Bioadhesive Hydrogels
First, we evaluated the viability, metabolic activity, and spreading of bone marrow mouse stromal cells (W-20-17[46]) encapsulated within the adhesives using
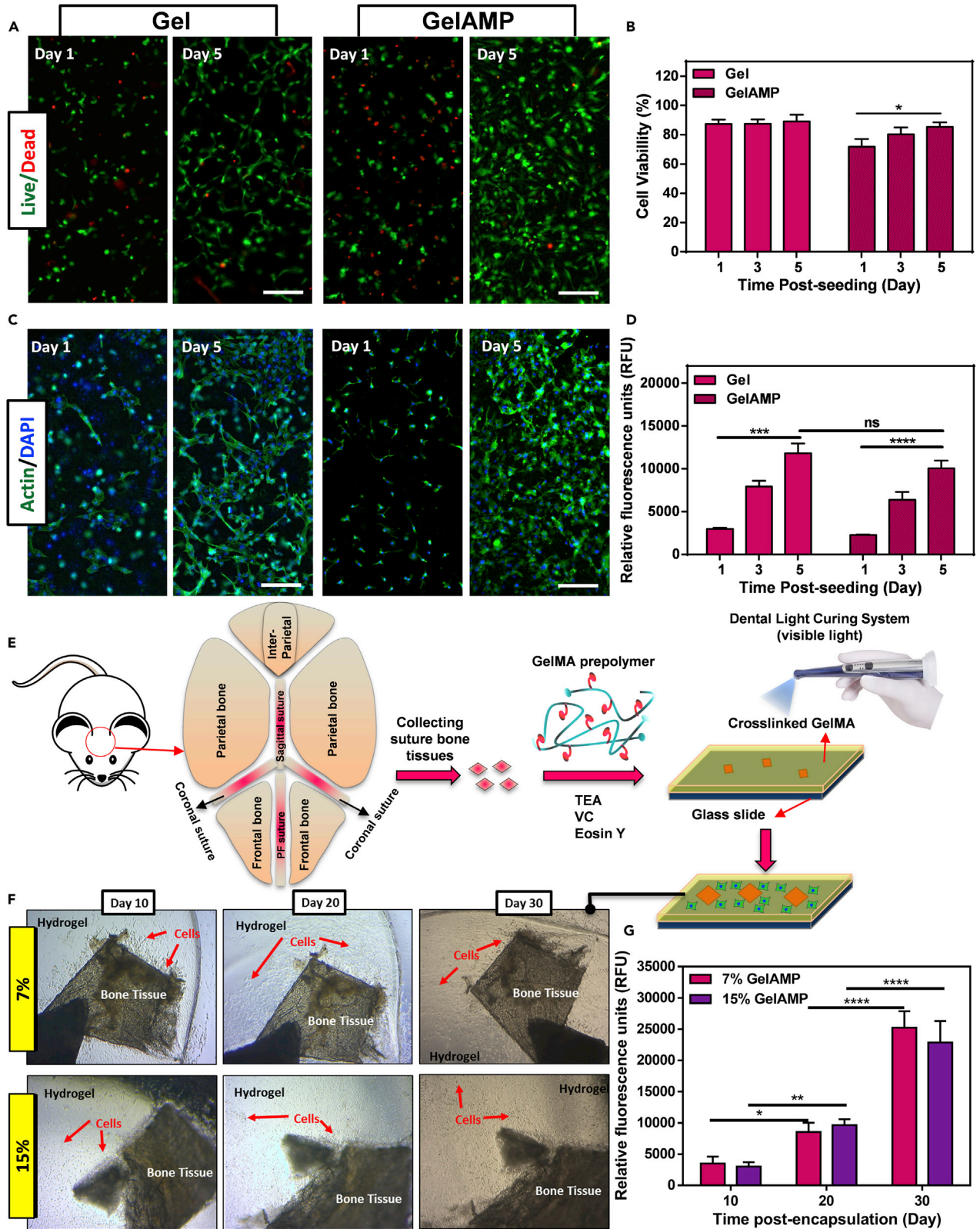
Figure 4. *In Vitro* 3D Encapsulation of W-20-17 Cells and Mouse Calvarial Bone Sutures inside the Bioadhesive Hydrogels

(A) Representative live/dead images of W-20-17 cells encapsulated within bioadhesive hydrogels with and without AMP after 1 and 5 days (scale bar: 200 μm).

(B) Quantification of viability of W-20-17 cells incorporated within hydrogels without (control) and with AMP (GelAMP) using live/dead assays on days 1, 3, and 5 post encapsulation.

(C) Representative phalloidin (green)/DAPI (blue)-stained images of cell-laden bioadhesives with and without AMP after 1 and 5 days (scale bar: 200 μm).

(D) Quantification of metabolic activity of W-20-17 cells encapsulated in hydrogels after 1, 3, and 5 days.

(E) Schematic diagram of the extraction and encapsulation of mouse calvarial bone sutures in 3D hydrogel network.

(F) Representative images of calvarial bone sutures encapsulated within 7% and 15% (w/v) bioadhesives to visualize growth and diffusion of cells on days 10, 20, and 30 post-encapsulation.

(G) Quantification of metabolic activity of migratory stromal cells from encapsulated bone sutures. Bioadhesive hydrogels were formed at 120 s visible light exposure time.

ns, not significant;*p < 0.05, **p < 0.01, ***p < 0.001, ****p < 0.0001.

live/dead and PrestoBlue assays, and F-actin/DAPI staining, respectively. Our results showed that cells encapsulated within the bioadhesives with and without AMP exhibited >90% viability after 5 days of culture (Figures 4A and 4B). In addition, the incorporation of AMP did not affect the viability of the encapsulated cells (Figures 4A and 4B). Moreover, F-actin/DAPI staining revealed that W-20-17 cells could attach and proliferate throughout the 3D network for both Gel and GelAMP adhesives up to 5 days of culture (Figure 4C). Furthermore, the metabolic activity of cells in GelAMP hydrogels increased consistently from 2,273 ± 66 relative fluorescence units (RFU) at day 1 to 10,041 ± 938 RFU at day 5 of culture (Figure 4D). In addition, there were no statistically significant differences between the metabolic activity of cells seeded on GelAMP and Gel adhesives (Figure 4D).

3D Encapsulation of Calvarial Bone Suture Explants within the Bioadhesives

We encapsulated the freshly isolated calvarial bone sutures in both 7% and 15% (w/v) hydrogels to evaluate the ability of the bioadhesives to support the proliferation and migration of stromal cells (Figure 4E). During the first week of encapsulation, no significant cell migration was observed. A week after encapsulation, cell (most likely suture-derived skeletal stem cells[47,48]) deployment out of the suture was observed, followed by proliferation and migration within the bioadhesive hydrogel (Figure 4F). The migratory and proliferative behavior of these cells was assessed for up to 30 days post-encapsulation (Figure 4F). The results showed that the metabolic activity of the encapsulated cells increased consistently for both 7% and 15% (w/v) bioadhesives (Figure 4G). For instance, the metabolic activity of the cells in 15% GelAMP (w/v) bioadhesives increased from 3,016 ± 678 RFU at day 10 to 22,869 ± 3,421 RFU at day 30 post encapsulation (Figure 4G). However, we did not observe any statistical difference between metabolic activity of the cells seeded within the 7% and 15% (w/v) bioadhesive hydrogels (Figure 4G).

Our results also indicated that the GelAMP bioadhesives did not elicit any cytotoxic response and could effectively support the growth of both W-20-17 and suture-derived skeletal stem cells *in vitro*. Previous studies have reported the development of different types of antimicrobial hydrogels based on the incorporation of metal or metal oxide nanoparticles.[24,49] However, the negative effect of metal oxide nanoparticles on cell viability greatly limits their application for the clinical management of PIDs.[49] In contrast, our results demonstrated that the cells could infiltrate and spread throughout GelAMP bioadhesives while also remaining proliferative and metabolically active.

Taken together, these results demonstrated that our bioadhesives could be used to form an adhesive and antimicrobial barrier that prevents bacterial growth and supports the proliferation of bone-competent cells *in vitro*. The ability of GelAMP

bioadhesives to eradicate or prevent infection at the implant site could not only be relevant to disinfect the affected area, but also to reduce inflammatory responses triggered by sustained microbial colonization. Moreover, the establishment of a cell-supportive microenvironment could promote the regeneration of the affected bone by endogenous progenitor cells that migrate into the wound site. Therefore, we next aimed to evaluate the ability of the bioadhesives to support bone regeneration *in vivo* using a calvarial defect model in mice.

In Vivo Application and Evaluation of the Bioadhesive Hydrogels

We investigated the ability of the bioadhesives to be delivered and formed *in situ* and to remain firmly attached to the wound area without the risk of displacement during the healing process. For this, we first created critically sized defects in mice calvaria using dental drills. The bioadhesive precursor solutions (7% and 15% [w/v]) were directly injected into the bone defects and photopolymerized using a commercial dental light curing unit (Figure 5A). Our results showed that the bioadhesives could remain at the site of application without any sign of displacement after 7 and 14 days of implantation (Figure 5B). In addition, histological assessment (using H&E) showed the complete sealing of the defect and a strong coherence between the bioadhesive and the native bone following application (Figure 5C). Moreover, the H&E images also revealed that bioadhesives with both formulations (7% and 15% [w/v]) could remain attached to the wound site up to 42 days after application (Figures 5D and 5E). At earlier time points (14 days post application), the formation of new autologous bone could be observed near the margin of the original defect (Figure S3). Calvarial defects in untreated control animals showed limited new bone formation at day 42 post application (Figure 5F). In contrast, histological staining revealed the formation of new bone for both 7% and 15% (w/v) bioadhesives (Figures 5D and 5E). Furthermore, the area covered by the newly formed bone was significantly larger for defects treated with 15% (w/v) hydrogels compared with 7% (w/v) hydrogels (Figure S3). This observation could be explained in part due to the increased structural integrity of bioadhesives with higher polymer concentration, which provided a more structurally stable scaffold to support bone regeneration and the ingrowth of the adjacent connective tissues (Figure 5E). These observations provided qualitative evidence that was indicative of the formation of new bone and the subsequent repair of the defect.

To perform a quantitative evaluation of new bone formation, we performed micro-computed tomography (μCT) on untreated defects as well as defects treated with bioadhesives synthesized using 7% and 15% (w/v) polymer concentrations at days 0, 28, and 42 post procedure (Figure 6). Our results showed that the untreated defects exhibited limited evidence of bone formation up to 28 and 42 days post procedure, with little decrease in the extension of the critical size (Figure 6A). At day 28, the defects treated with the 15% (w/v) hydrogels showed significantly higher bone formation than 7% (w/v) hydrogels and the untreated groups. At day 42, a significant amount of new bone was observed for defects treated with 15% (w/v) hydrogels (Figure 6A). In addition, on days 28 and 42, the bone surface area (BS) and the bone volume (BV) for 15% (w/v) hydrogels were shown to be significantly higher than that of untreated and 7% (w/v) groups (Figures 6B and 6C). For instance, at day 42, the BS for 15% (w/v) hydrogels corresponded to 2.96 ± 0.46 mm^2, which was significantly higher than those of the untreated controls (i.e., 1.03 ± 0.63 mm^2) and 7% (w/v) hydrogels (i.e., 1.40 ± 0.53 mm^2) (Figure 6B). Moreover, the highest BV was observed for 15% (w/v) bioadhesives (i.e., 7.16 ± 1.65 mm^3), which was significantly higher than those of untreated (i.e., 2.76 ± 1.03 mm^3) and 7% (w/v) bioadhesives (i.e., 4.45 ± 0.72 mm^3) (Figure 6C). Statistical analysis indicated that both
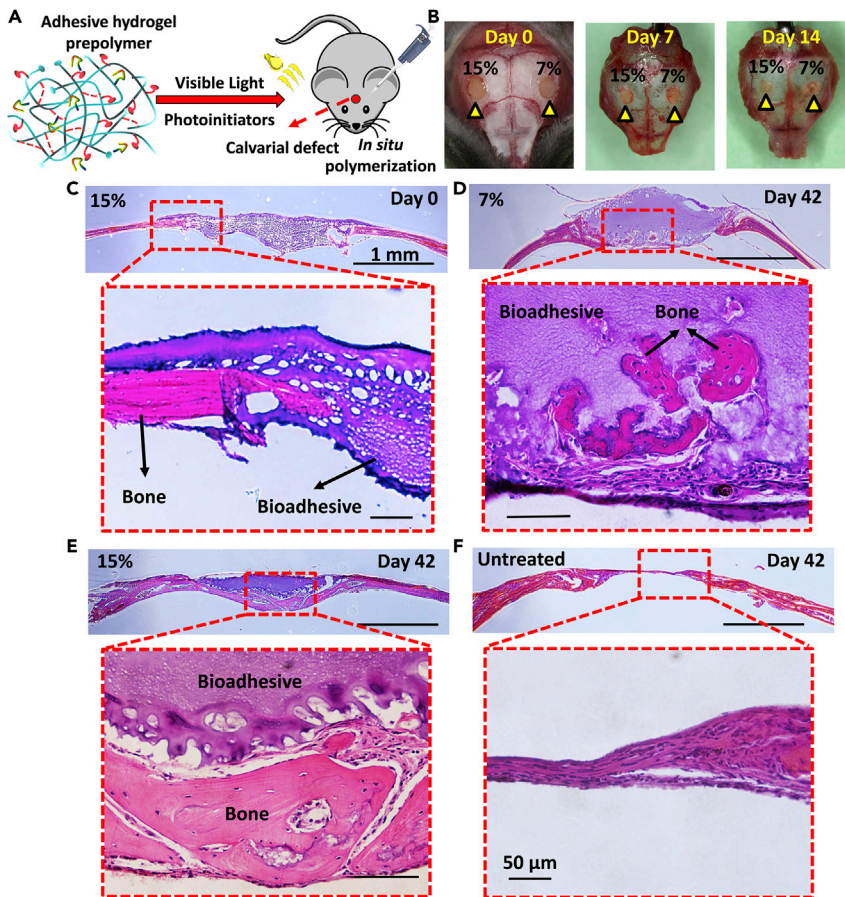
Figure 5. *In Vivo* Evaluation of the Bioadhesive Hydrogels Using a Mouse Calvarial Defect Model

(A) Schematic diagram of *in situ* application of bioadhesive hydrogels in a mouse calvarial defect model.

(B) Bioadhesive hydrogels (7% and 15%) were delivered to artificially created bone defects in mouse calvaria (yellow arrowheads), and photopolymerized for 1 min using a commercially available dental curing light. Seven and 14 days after implantation, samples remained in place, without any sign of detachment.

(C–F) Histological evaluation (H&E staining) of the 15% (w/v) bioadhesives at day 0 post implantation (C). Representative H&E images for (D) 7% (w/v) and (E) 15% (w/v) bioadhesive treatments, and (F) untreated sample after 42 days of implantation (scale bars: 1 mm and 50 μm).

the concentration of the biopolymer and the treatment time had a significant effect on BV and BS. For instance, the BS and BV increased 1.27- and 1.66-fold, respectively, at 28 and 42 days post procedure, which was indicative of sustained bone regeneration throughout the experiment (Figures 6B and 6C).

The higher degree of bone regeneration observed for 15% (w/v) bioadhesive could be due in part to the direct contribution of the enhanced mechanical properties of hydrogels with higher polymer concentrations.[36] For instance, Huebsch et al. demonstrated that the contribution of matrix elasticity to new bone formation *in vivo* is highly correlated with mechanically induced osteogenesis.[36] They reported that the BV and mineral density obtained for hydrogels with elasticities in the range of 60 kPa was significantly higher than those with 5-kPa or 120-kPa moduli.[36] In our study, 15% (w/v) bioadhesives, which exhibited elastic and compressive modulus corresponding to 53.0 ± 10.3 kPa and 52.2 ± 4.7 kPa (Figure 1B), respectively, could potentially enable mechanically induced
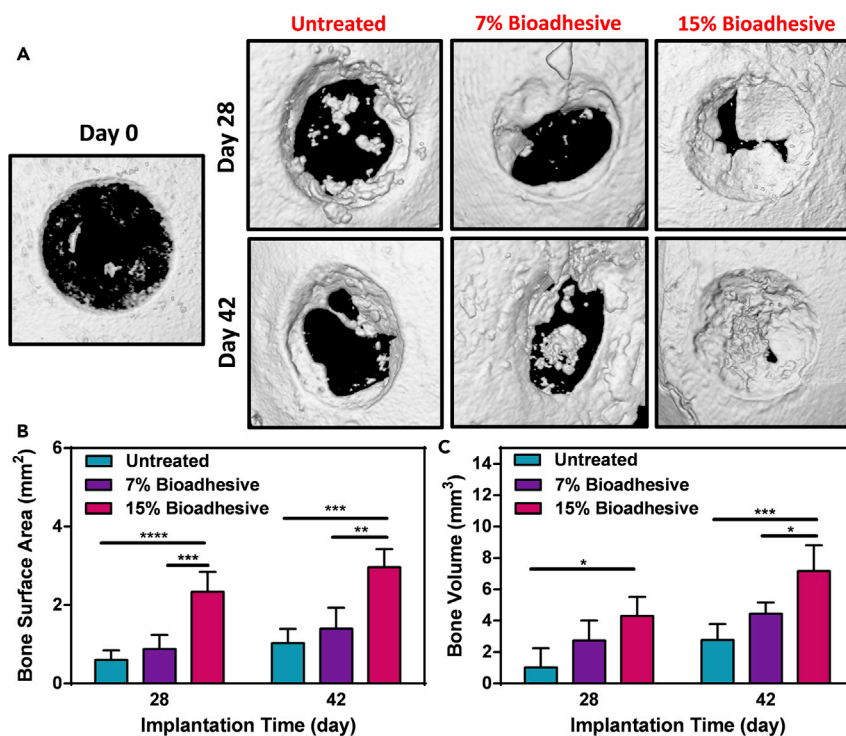
Figure 6. Quantitative Evaluation of New Bone Formation Using μCT Analysis

(A) Representative μCT images for untreated defect, and defects treated with 7% and 15% bioadhesives on days 28 and 42 post implantation.

(B and C) Quantitative analysis of bone surface area (B) and bone volume (C). Data are presented as mean ± SD (*p < 0.05, **p < 0.01, ***p < 0.001, ****p < 0.0001; n = 5).

osteogenesis and thus promote the formation of new bone *in vivo*. However, the clinical efficacy of antimicrobial bioadhesives for the treatment of patients with advanced PI could be limited due to the lack of a bona fide osteoinductive strategy. Although previous groups have reported the development of regenerative bioadhesives, they often rely on the use of growth factors,[50,51] stem cells,[36,52] and other bioactive molecules.[53,54] These methods often suffer from clinical limitations and drawbacks.[55,56] Due to these limitations, in our future work we will introduce a cell-/growth factor-free strategy by the incorporation of alternative osteoinductive strategies such as nanosilicates[57] into antimicrobial bioadhesives, which could constitute an attractive platform for the development of osteoinductive and antimicrobial bioadhesives for the treatment of PIDs.

Conclusion

The clinical management of PIDs still constitutes significant challenges for clinicians and researchers in the dentistry field. In this study, we engineered antimicrobial hydrogel bioadhesives for the treatment of PIDs. The hydrogel precursors could be readily delivered and photocrosslinked *in situ* using commercial dental curing systems. These bioadhesives exhibited tunable mechanical stiffness and elasticity, and comparatively higher adhesive strength to implant and oral surfaces than commercial adhesives. In addition, the bioadhesives showed high antimicrobial activity *in vitro* against *P. gingivalis*, a pathogenic bacterium associated with the onset and progression of PIDs. *In vitro* and *ex vivo* studies demonstrated that the bioadhesives were highly cytocompatible and could provide a suitable microenvironment for migratory stromal cells deployed from encapsulated bone sutures. Furthermore, *in vivo* studies showed that the bioadhesives could promote bone regeneration

by supporting the growth of migratory progenitor cells. Taken together, our results demonstrated the remarkable potential of our bioadhesive hydrogels to be used as adhesive, antimicrobial, and cell-supportive barriers that can support tissue healing and bone regeneration *in vivo* for the treatment of PIDs.

EXPERIMENTAL PROCEDURES

Synthesis of Photocrosslinkable Bioadhesive Prepolymers

Gelatin methacryloyl was synthesized as previously described.[58–60] In brief, 10 g of gelatin from cold water fish skin (Sigma-Aldrich) was dissolved in 100 mL of DPBS at 60°C for 30 min. Next, 8% (v/v) methacrylic anhydride (Sigma-Aldrich) was added to the solution dropwise under vigorous stirring at 60°C for another 3 h. The solution was then diluted with 300 mL of DPBS to stop the reaction and dialyzed (Spectrum Laboratories, molecular weight cutoff = 12–14 kDa) in a deionized water bath at 50°C for 5 days to remove the unreacted methacrylic anhydride. The resulting solution was filtered and lyophilized for 4 days.

Fabrication of Bioadhesive Hydrogels

Adhesive hydrogels (Gel) were formed by first dissolving different concentrations of gelatin methacryloyl (7% and 15% [w/v]) in the photoinitiator solution containing TEA (1.88% [w/v]) and VC (1.25% [w/v]) in distilled water at room temperature. A separate solution of Eosin Y disodium salt (0.5 mM) was also prepared in distilled water. The biopolymer/TEA/VC solutions were then mixed with Eosin Y prior to crosslinking to form the final precursor solution. To form the hydrogels, we pipetted 70 mL of the precursor solution into polydimethylsiloxane (PDMS) cylindrical molds (diameter: 6 mm; height: 2.5 mm) for compressive tests, or rectangular molds (12 × 5 × 1 mm) for tensile tests. Lastly, the solutions were photocrosslinked upon exposure to visible light (420–480 nm) for 120 s, using a VALO dental light curing unit (Ultradent Products). GelAMP hydrogels were formed by dissolving 0.2% (w/v) AMP Tet213 (CSC Scientific) in TEA/VC/Eosin Y photoinitiator solution. The lyophilized biopolymers were then dissolved in the resulting solution and photocrosslinked as described above.

Mechanical Properties

The tensile and compressive properties of the hydrogel adhesives were evaluated using an Instron 5542 mechanical tester, as described previously[25] (Supplemental Experimental Procedures).

In Vitro Swellability and Degradation

The *in vitro* swellability (24 h) and degradation (14 days) of bioadhesives were performed in DPBS as described previously[25] (Supplemental Experimental Procedures).

In Vitro Adhesion

In Vitro *Wound Closure*

Wound closure test was performed on both porcine gingiva and skin tissues using a modified ASTM F2458-05 test, as described previously.[25] In brief, the porcine gingiva was isolated from fresh porcine mandible. Tissues were then cut into 1 × 2-cm pieces and kept moist prior to the test. The tissues were glued onto two precut glass slides (20 × 30 mm), then 50 μL of precursor solution was pipetted and crosslinked using a dental light curing system to form the adhesives. The samples were then placed between the Instron tensile grips and the ultimate adhesive strength was calculated at break (n ≥ 5). Similarly, 50 μL of the commercial adhesive material was tested as a control.

In Vitro *Lap Shear*

The lap shear strength of the bioadhesives and a commercial adhesive, CoSEAL (Baxter, Deerfield, IL, USA), was determined according to a modified ASTM test (F2255-05). Both titanium and glass slides were used as the substrates. Glass slides (10 × 30 mm) were coated with gelatin solution and dried at 37°C. For adhesive tests on titanium, a piece of titanium (10 × 10 mm) was attached to a glass slide and 10 μL of the precursor solution was photocrosslinked between the titanium and the gelatin-coated glass slide. The lap shear strength of the adhesives was then measured under tensile stress at a rate of 1 mm/min using an Instron mechanical tester. The ultimate stress was reported as shear strength of the bioadhesives (n ≥ 5). Similarly, 10 μL of the commercial adhesive material was tested as a control.

In Vitro *Burst Pressure*

The burst pressures of the bioadhesives and CoSEAL were determined using a modified ASTM (F2392-04) test as described previously.[24] A piece of porcine intestine was fixed between the stainless-steel annuli of a custom-designed burst pressure setup. A 2-mm defect was then created on the center of the tissue. Next, 30 μL precursor solution was applied to the defect site and crosslinked using a dental light curing system. Air pressure was then applied to the sealed tissue and the maximum resistance pressure was recorded as burst pressure (n ≥ 5). Similarly, 30 μL of the commercial adhesive material was tested as a control.

In Vitro Antimicrobial Properties of Adhesive Hydrogels

P. gingivalis (clinical isolate A7436[61]) was used to evaluate the antimicrobial properties of GelAMP bioadhesives. *P. gingivalis* was grown on 5% sheep's blood agar plates supplemented with hemin and vitamin K (H & K) in an anaerobic system (5% H_2, 15% CO_2, 80% N_2) at 37°C for 7 days. The bacteria colonies were then transferred to Wilkins-Chalgren Anaerobe Broth (Oxoid) medium to prepare a 10^8 CFU/mL bacterial solution. For antimicrobial tests, 1 mL of a 10^8 CFU/mL bacteria solution was seeded on cylindrical hydrogels with and without AMP (0% and 0.2% [w/v] or 1.34 mM) in 24-well plates. After 72 h of anaerobic incubation, the samples were removed from the medium and washed gently three times with DPBS. Next, each sample was placed in 1 mL of DPBS and vortexed for 15 min to release bacteria from within the scaffold. The solutions were then logarithmically diluted to 10^{-1}, 10^{-3}, and 10^{-4} dilutions. A 30-μL volume of each dilution was then seeded on sheep's blood agar plates with H & K and incubated for 5 days. The number of colonies was counted and reported for each sample (n = 4). For SEM imaging, hydrogels were removed from the medium and washed three times with DPBS. The samples were then fixed in a solution of 2.5% (v/v) glutaraldehyde (Sigma-Aldrich) and 4% (v/v) paraformaldehyde (Sigma-Aldrich) in DPBS for 30 min. After fixation, the samples were gently washed three times with DPBS and dehydrated using a serially diluted ethanol solution in water (30%, 50%, 70%, 90%, and 100% [v/v]). The samples were then dried using a critical point dryer. Lastly, the samples were mounted on aluminum SEM stubs, sputter coated with 6 nm of gold/palladium, and imaged by a Hitachi S-4800 scanning electron microscope (n = 3).

In Vitro Cell Studies

Cell Lines

Bone marrow mouse stromal cells (W-20-17) were cultured at 37°C and 5% CO_2 in Minimum Essential Medium (MEM) Alpha medium without ascorbic acid (Gibco), containing 10% (v/v) fetal bovine serum (FBS) and 1% (v/v) penicillin/streptomycin (Gibco).

2D Cell Seeding on Adhesive Hydrogels

Hydrogels were formed by pipetting 10 μL of precursor solution between a 3-(trimethoxysilyl) propyl methacrylate (TMSPMA; Sigma-Aldrich)-coated glass slide (10 × 10 mm) and a glass coverslip separated with a 100-μm spacer. Bioadhesive hydrogels were photocrosslinked using visible light for 60 s. The hydrogels were seeded with W-20-17 cells (5×10^6 cells/mL) and kept at 37°C, 5% CO_2 for 5 days.[60]

3D Cell Encapsulation within the Engineered Hydrogels

For 3D cell encapsulation, a suspension of W-20-17 cells (5×10^6 cells/mL) was prepared by trypsinization and resuspension in MEM alpha medium. The cell suspension was centrifuged to form a cell pellet and the medium was discarded. A hydrogel precursor containing 7% bioadhesive was prepared in culture medium containing TEA/VC/Eosin Y and mixed with the cell pellet. Hydrogels were formed by pipetting 10 μL of the precursor solution between a TMSPMA-coated glass slide and a glass coverslip separated with a 100-μm spacer, and photocrosslinking upon exposure to visible light for 60 s. Lastly, the glass slides with the encapsulated W-20-17 cells were placed in 24-well plates and incubated in MEM alpha at 37°C and 5% CO_2.

Cell Viability, Proliferation, and Spreading

A calcein AM/ethidium homodimer-1 live/dead kit (Invitrogen) was used to evaluate cell viability as described previously.[62] Cell proliferation and metabolic activity was determined using a commercial PrestoBlue assay (Fisher) on days 0, 1, 3, and 5 as described previously.[25] Cell spreading in 2D and 3D cultures was evaluated via fluorescent staining of F-actin microfilaments and cell nuclei[25,63] (Supplemental Experimental Procedures) ($n \geq 3$).

Animal Studies

Calvarial Bone Suture Tissue Extraction and Encapsulation into the Gels

All animal experiments were performed according to the Guide for the Care and Use of Laboratory Animals (IACUC approval IS00000535) at Harvard School of Dental Medicine. For all experiments, 7- to 8-week-old wild-type house mice (*Mus musculus*) were used. To obtain the calvarial bone sutures, we first euthanized the mice by CO_2 inhalation, before carrying out cervical dislocation. After decapitation, the head was cleaned using 70% ethanol. A cut was then created through the skin at the base of the skull using a surgical blade. Next, an incision was made starting at the nose bridge and ending at the base of the skull followed by removal of the skin from the top of the head. The calvaria was then cut and transferred to a Petri dish with DPBS. After washing with DPBS, the soft tissues were removed using tweezers and the sutures were isolated using scissors. The isolated tissues were chopped into small fragments of 1–2 mm^2 and quickly transferred to ice-cold cell culture medium prior to use. For encapsulation, the suture fragments were placed on a flat Petri dish, in between two spacers (500 μm). Next, 70 μL of the bioadhesive precursor was pipetted on the tissue samples and covered by a glass coverslip. The samples were then photocrosslinked for 2 min using a dental curing light. Samples were removed from Petri dishes and placed in 12-well tissue culture plates. Next, 2 mL of MEM Alpha medium, containing 10% (v/v) FBS and 1% (v/v) penicillin/streptomycin, was added to each well and the samples were incubated at 37°C for up to 30 days. The samples were imaged using a Zeiss Primo Vert inverted microscope, and the cell metabolic activity was evaluated as described previously ($n \geq 3$).

Mouse Calvarial Bone Defect Model

Male and female mice were assigned randomly to all experimental groups. After general anesthesia, 2-mm round defects were made with a surgical bur on right

and left parietal bone of mice. Next, 10 μL of the precursor solution was injected in the defect sites (7% and 15% [w/v]) and photopolymerized using a dental light curing unit for 1 min. After anatomical wound closure, the animals recovered from anesthesia. At each time point, the animals were euthanized by CO_2 inhalation, followed by cervical dislocation. After euthanasia, calvarial tissues were collected for μCT and histological analysis (Supplemental Experimental Procedures) (n ≥ 3).

Statistical Analysis

All data are presented as mean ± standard deviation (*p < 0.05, **p < 0.01, ***p < 0.001, and ****p < 0.0001). T test, one-way ANOVA, or two-way ANOVA followed by Tukey's test were performed using the GraphPad Prism 6.0 Software.

SUPPLEMENTAL INFORMATION

Supplemental Information can be found online at https://doi.org/10.1016/j.matt.2019.07.019.

AUTHOR CONTRIBUTIONS

E.S.S., N.A., G.I., and A.K. designed the experiments. E.S.S. synthesized the bioadhesive hydrogels. E.S.S. conducted the physical characterization and adhesion experiments. E.S.S. conducted the *in vitro* cytocompatibility tests. E.S.S. and D.N. performed the *in vitro* antimicrobial test. E.S.S., R.P.L., and S.H.B. extracted and encapsulated the calvarial bone sutures. E.S.S. and Z.A. conducted the *in vivo* experiments, and E.S.S. performed histopathological analysis. All the authors contributed to the interpretation of the results and data analysis. The paper was written by E.S.S. and R.P.L., and was revised and corrected by N.A., G.I., and A.K.. The project was supervised by N.A.

DECLARATION OF INTERESTS

E.S.S. and N.A. are inventors on a U.S. Provisional Patent Application (No. 62/860,939), entitled "Osteoinductive modified gelatin hydrogels and methods of making and using the same," filed by UCLA's Technology Development Group with the United States Patent and Trademark Office. The other authors declare no competing interests.

REFERENCES

1. Poli, P.P., Cicciu, M., Beretta, M., and Maiorana, C. (2017). Peri-implant mucositis and peri-implantitis: a current understanding of their diagnosis, clinical implications, and a report of treatment using a combined therapy approach. J. Oral Implantol. *43*, 45–50.

2. Berglundh, T., Armitage, G., Araujo, M.G., Avila-Ortiz, G., Blanco, J., Camargo, P.M., Chen, S., Cochran, D., Derks, J., and Figuero, E. (2018). Peri-implant diseases and conditions: consensus report of workgroup 4 of the 2017 world workshop on the classification of periodontal and peri-implant diseases and conditions. J. Clin. Periodontol. *45*, S286–S291.

3. Renvert, S., Persson, G.R., Pirih, F.Q., and Camargo, P.M. (2018). Peri-implant health, peri-implant mucositis, and peri-implantitis: case definitions and diagnostic considerations. J. Clin. Periodontol. *45*, S278–S285.

4. American Academy of Periodontology (2013). Peri-implant mucositis and peri-implantitis: a

current understanding of their diagnoses and clinical implications. J. Periodontol. 84, 436–443.

5. Costa, F.O., Takenaka-Martinez, S., Cota, L.O., Ferreira, S.D., Silva, G.L., and Costa, J.E. (2012). Peri-implant disease in subjects with and without preventive maintenance: a 5-year follow-up. J. Clin. Periodontol. 39, 173–181.

6. Renvert, S., Roos-Jansaker, A.M., and Claffey, N. (2008). Non-surgical treatment of peri-implant mucositis and peri-implantitis: a literature review. J. Clin. Periodontol. 35, 305–315.

7. Mombelli, A., Feloutzis, A., Bragger, U., and Lang, N.P. (2001). Treatment of peri-implantitis by local delivery of tetracycline. Clinical, microbiological and radiological results. Clin. Oral Implants Res. 12, 287–294.

8. Renvert, S., Roos-Jansåker, A.M., and Claffey, N. (2008). Non-surgical treatment of peri-implant mucositis and peri-implantitis: a literature review. J. Clin. Periodontol. 35, 305–315.

9. Grusovin, M.G., Coulthard, P., Worthington, H.V., George, P., and Esposito, M. (2010). Interventions for replacing missing teeth: maintaining and recovering soft tissue health around dental implants. Cochrane Database Syst. Rev. CD003069. https://doi.org/10.1002/14651858.CD003069.pub4.

10. Diz, P., Scully, C., and Sanz, M. (2013). Dental implants in the medically compromised patient. J. Dent. 41, 195–206.

11. Esposito, M., Coulthard, P., Oliver, R., Thomsen, P., and Worthington, H. (2003). Antibiotics to prevent complications following dental implant treatment. Cochrane Database Syst. Rev. CD004152. https://doi.org/10.1002/14651858.CD004152.

12. Frederic, L.J., Michel, B., and Selena, T. (2018). Oral microbes, biofilms and their role in periodontal and peri-implant diseases. Materials (Basel) 11, https://doi.org/10.3390/ma11101802.

13. Derks, J., and Tomasi, C. (2015). Peri-implant health and disease. A systematic review of current epidemiology. J. Clin. Periodontol. 42 (Suppl 16), S158–S171.

14. Kinane, D.F. (2001). Causation and pathogenesis of periodontal disease. Periodontol 2000, 8–20.

15. Heitz-Mayfield, L.J.A., and Salvi, G.E. (2018). Peri-implant mucositis. J. Periodontol. 89 (Suppl 1), S257–S266.

16. Gottlow, J., Nyman, S., Karring, T., and Lindhe, J. (1984). New attachment formation as the result of controlled tissue regeneration. J. Clin. Periodontol. 11, 494–503.

17. Nyman, S. (1991). Bone regeneration using the principle of guided tissue regeneration. J. Clin. Periodontol. 18, 494–498.

18. Ivanovski, S., Vaquette, C., Gronthos, S., Hutmacher, D.W., and Bartold, P.M. (2014). Multiphasic scaffolds for periodontal tissue engineering. J. Dent. Res. 93, 1212–1221.

19. Sheikh, Z., Qureshi, J., Alshahrani, A.M., Nassar, H., Ikeda, Y., Glogauer, M., and Ganss, B. (2017). Collagen based barrier membranes for periodontal guided bone regeneration applications. J. Odontology 105, 1–12.

20. Larsson, L., Decker, A.M., Nibali, L., Pilipchuk, S.P., Berglundh, T., and Giannobile, W.V. (2016). Regenerative medicine for periodontal and peri-implant diseases. J. Dent. Res. 95, 255–266.

21. Sam, G., and Pillai, B.R. (2014). Evolution of barrier membranes in periodontal regeneration—"Are the third generation membranes really here?". J. Clin. Diagn. Res. 8, ZE14–17.

22. Sculean, A., Nikolidakis, D., Nikou, G., Ivanovic, A., Chapple, I.L., and Stavropoulos, A. (2015). Biomaterials for promoting periodontal regeneration in human intrabony defects: a systematic review. Periodontol 2000, 182–216.

23. Kao, R.T., Nares, S., and Reynolds, M.A. (2015). Periodontal regeneration—intrabony defects: a systematic review from the AAP Regeneration Workshop. J. Periodontol. 86, S77–S104.

24. Annabi, N., Rana, D., Shirzaei Sani, E., Portillo-Lara, R., Gifford, J.L., Fares, M.M., Mithieux, S.M., and Weiss, A.S. (2017). Engineering a sprayable and elastic hydrogel adhesive with antimicrobial properties for wound healing. Biomaterials 139, 229–243.

25. Shirzaei Sani, E., Portillo-Lara, R., Spencer, A., Yu, W., Geilich, B.M., Noshadi, I., Webster, T.J., and Annabi, N. (2018). Engineering adhesive and antimicrobial hyaluronic acid/elastin-like polypeptide hybrid hydrogels for tissue engineering applications. ACS Biomater. Sci. Eng. 4, 2528–2540.

26. Athirasala, A., Tahayeri, A., Thrivikraman, G., Franca, C.M., Monteiro, N., Tran, V., Ferracane, J., and Bertassoni, L.E. (2018). A dentin-derived hydrogel bioink for 3D bioprinting of cell laden scaffolds for regenerative dentistry. Biofabrication 10, 024101.

27. Monteiro, N., Thrivikraman, G., Athirasala, A., Tahayeri, A., França, C.M., Ferracane, J.L., and Bertassoni, L.E. (2018). Photopolymerization of cell-laden gelatin methacryloyl hydrogels using a dental curing light for regenerative dentistry. Dent. Mater. 34, 389–399.

28. Sinha, R.P., and Häder, D.-P. (2002). UV-induced DNA damage and repair: a review. Photochem. Photobiol. Sci. 1, 225–236.

29. Kappes, U.P., Luo, D., Potter, M., Schulmeister, K., and Rünger, T.M. (2006). Short-and long-wave UV light (UVB and UVA) induce similar mutations in human skin cells. J. Invest. Dermatol. 126, 667–675.

30. Wang, Z., Abdulla, R., Parker, B., Samanipour, R., Ghosh, S., and Kim, K. (2015). A simple and high-resolution stereolithography-based 3D bioprinting system using visible light crosslinkable bioinks. Biofabrication 7, 045009.

31. Assmann, A., Vegh, A., Ghasemi-Rad, M., Bagherifard, S., Cheng, G., Sani, E.S., Ruiz-Esparza, G.U., Noshadi, I., Lassaletta, A.D., Gangadharan, S., et al. (2017). A highly adhesive and naturally derived sealant. Biomaterials 140, 115–127.

32. Soucy, J.R., Shirzaei Sani, E., Portillo Lara, R., Diaz, D., Dias, F., Weiss, A.S., Koppes, A.N., Koppes, R.A., and Annabi, N. (2018). Photocrosslinkable gelatin/tropoelastin hydrogel adhesives for peripheral nerve repair. Tissue Eng. A 24, 1393–1405.

33. Shih, H., and Lin, C.C. (2013). Visible-light-mediated thiol-Ene hydrogelation using eosin-Y as the only photoinitiator. Macromol. Rapid Commun. 34, 269–273.

34. Noshadi, I., Hong, S., Sullivan, K.E., Shirzaei Sani, E., Portillo-Lara, R., Tamayol, A., Shin, S.R., Gao, A.E., Stoppel, W.L., Black Iii, L.D., et al. (2017). In vitro and in vivo analysis of visible light crosslinkable gelatin methacryloyl (GelMA) hydrogels. Biomater. Sci. 5, 2093–2105.

35. Kazemzadeh-Narbat, M., Kindrachuk, J., Duan, K., Jenssen, H., Hancock, R.E., and Wang, R. (2010). Antimicrobial peptides on calcium phosphate-coated titanium for the prevention of implant-associated infections. Biomaterials 31, 9519–9526.

36. Huebsch, N., Lippens, E., Lee, K., Mehta, M., Koshy, S.T., Darnell, M.C., Desai, R.M., Madl, C.M., Xu, M., and Zhao, X. (2015). Matrix elasticity of void-forming hydrogels controls transplanted-stem-cell-mediated bone formation. Nat. Mater. 14, 1269.

37. Peh, K.K., and Wong, C.F. (1999). Polymeric films as vehicle for buccal delivery: swelling, mechanical, and bioadhesive properties. J. Pharm. Pharm. Sci. 2, 53–61.

38. Nasajpour, A., Ansari, S., Rinoldi, C., Rad, A.S., Aghaloo, T., Shin, S.R., Mishra, Y.K., Adelung, R., Swieszkowski, W., and Annabi, N. (2018). A multifunctional polymeric periodontal membrane with osteogenic and antibacterial characteristics. Adv. Funct. Mater. 28, 1703437.

39. Cheng, H., Yue, K., Kazemzadeh-Narbat, M., Liu, Y., Khalilpour, A., Li, B., Zhang, Y.S., Annabi, N., and Khademhosseini, A. (2017). Mussel-inspired multifunctional hydrogel coating for prevention of infections and enhanced osteogenesis. ACS Appl. Mater. Interfaces 9, 11428–11439.

40. Purk, J.H., Healy, M., Dusevich, V., Glaros, A., and Eick, J.D. (2006). In vitro microtensile bond strength of four adhesives tested at the gingival and pulpal walls of Class II restorations. J. Am. Dent. Assoc. 137, 1414–1418.

41. Sofan, E., Sofan, A., Palaia, G., Tenore, G., Romeo, U., and Migliau, G. (2017). Classification review of dental adhesive systems: from the IV generation to the universal type. Ann. Stomatol. (Roma) 8, 1–17.

42. Khurshid, Z., Zafar, M.S., Naseem, M., Khan, R.S., and Najeeb, S. (2018). Human oral defensins antimicrobial peptides: a future promising antimicrobial drug. Curr. Pharm. Des. 24, 1130–1137.

43. Mallapragada, S., Wadhwa, A., and Agrawal, P. (2017). Antimicrobial peptides: the miraculous biological molecules. J. Indian Soc. Periodontol. 21, 434–438.

44. Shi, J., Liu, Y., Wang, Y., Zhang, J., Zhao, S., and Yang, G. (2015). Biological and immunotoxicity evaluation of antimicrobial peptide-loaded coatings using a layer-by-layer process on titanium. Sci. Rep. 5, 16336.

45. Chen, J., Zhu, Y., Song, Y., Wang, L., Zhan, J., He, J., Zheng, J., Zhong, C., Shi, X., and Liu, S. (2017). Preparation of an antimicrobial surface by direct assembly of antimicrobial peptide with its surface binding activity. J. Mater. Chem. B 5, 2407–2415.

46. Thies, R.S., Bauduy, M., Ashton, B.A., Kurtzberg, L., Wozney, J.M., and Rosen, V. (1992). Recombinant human bone morphogenetic protein-2 induces osteoblastic differentiation in W-20-17 stromal cells. Endocrinology 130, 1318–1324.

47. Maruyama, T., Jeong, J., Sheu, T.-J., and Hsu, W. (2016). Stem cells of the suture mesenchyme in craniofacial bone development, repair and regeneration. Nat. Commun. 7, https://doi.org/10.1038/ncomms10526.

48. Wilk, K., Yeh, S.-C.A., Mortensen, L.J., Ghaffarigarakani, S., Lombardo, C.M., Bassir, S.H., Aldawood, Z.A., Lin, C.P., and Intini, G. (2017). Postnatal calvarial skeletal stem cells expressing PRX1 reside exclusively in the calvarial sutures and are required for bone regeneration. Stem Cell Reports 8, 933–946.

49. Wahid, F., Zhong, C., Wang, H.-S., Hu, X.-H., and Chu, L.-Q.J.P. (2017). Recent advances in antimicrobial hydrogels containing metal ions and metals/metal oxide nanoparticles. Polymers (Basel) 9, 636.

50. Patterson, J., Siew, R., Herring, S.W., Lin, A.S., Guldberg, R., and Stayton, P.S. (2010). Hyaluronic acid hydrogels with controlled degradation properties for oriented bone regeneration. Biomaterials 31, 6772–6781.

51. Gibbs, D.M., Black, C.R., Dawson, J.I., and Oreffo, R.O. (2016). A review of hydrogel use in fracture healing and bone regeneration. J. Tissue Eng. Regen. Med. 10, 187–198.

52. Chamieh, F., Collignon, A.-M., Coyac, B.R., Lesieur, J., Ribes, S., Sadoine, J., Llorens, A., Nicoletti, A., Letourneur, D., and Colombier, M.-L. (2016). Accelerated craniofacial bone regeneration through dense collagen gel scaffolds seeded with dental pulp stem cells. Sci. Rep. 6, 38814.

53. Nguyen, M.K., Jeon, O., Dang, P.N., Huynh, C.T., Varghai, D., Riazi, H., McMillan, A., Herberg, S., and Alsberg, E. (2018). RNA interfering molecule delivery from in situ forming biodegradable hydrogels for enhancement of bone formation in rat calvarial bone defects. Acta Biomater. 75, 105–114.

54. Kyllönen, L., D'Este, M., Alini, M., and Eglin, D. (2015). Local drug delivery for enhancing fracture healing in osteoporotic bone. Acta Biomater. 11, 412–434.

55. Woo, E.J. (2012). Adverse events reported after the use of recombinant human bone morphogenetic protein 2. J. Oral Maxillofac. Surg. 70, 765–767.

56. Mesfin, A., Buchowski, J.M., Zebala, L.P., Bakhsh, W.R., Aronson, A.B., Fogelson, J.L., Hershman, S., Kim, H.J., Ahmad, A., and Bridwell, K.H. (2013). High-dose rhBMP-2 for adults: major and minor complications: a study of 502 spine cases. J. Bone Joint Surg. Am. 95, 1546–1553.

57. Wang, Y., Cui, W., Chou, J., Wen, S., Sun, Y., and Zhang, H. (2018). Electrospun nanosilicates-based organic/inorganic nanofibers for potential bone tissue engineering. Colloids Surf. B Biointerfaces 172, 90–97.

58. Uehara, M., Li, X., Sheikhi, A., Zandi, N., Walker, B., Saleh, B., Banouni, N., Jiang, L., Ordikhani, F., Dai, L., et al. (2019). Anti-IL-6 eluting immunomodulatory biomaterials prolong skin allograft survival. Sci. Rep. 9, 6535.

59. Walker, B.W., Lara, R.P., Yu, C., Sani, E.S., Kimball, W., Joyce, S., and Annabi, N.J.B. (2019). Engineering a naturally-derived adhesive and conductive cardiopatch. Biomaterials 207, 89–101.

60. Sani, E.S., Kheirkhah, A., Rana, D., Sun, Z., Foulsham, W., Sheikhi, A., Khademhosseini, A., Dana, R., and Annabi, N. (2019). Sutureless repair of corneal injuries using naturally derived bioadhesive hydrogels. Sci. Adv. 5, eaav1281.

61. Papathanasiou, E., Kantarci, A., Konstantinidis, A., Gao, H., and Van Dyke, T. (2016). SOCS-3 regulates alveolar bone loss in experimental periodontitis. J. Dent. Res. 95, 1018–1025.

62. Annabi, N., Zhang, Y.-N., Assmann, A., Sani, E.S., Cheng, G., Lassaletta, A.D., Vegh, A., Dehghani, B., Ruiz-Esparza, G.U., and Wang, X. (2017). Engineering a highly elastic human protein–based sealant for surgical applications. Sci. Transl. Med. 9, eaai7466.

63. Noshadi, I., Walker, B.W., Portillo-Lara, R., Shirzaei Sani, E., Gomes, N., Aziziyan, M.R., and Annabi, N. (2017). Engineering biodegradable and biocompatible bio-ionic liquid conjugated hydrogels with tunable conductivity and mechanical properties. Sci. Rep. 7, 4345.